Resistive cooling of ions' center-of-mass energy in a Penning trap on millisecond time scales

Markus Kiffer [*] and Stefan Ringleb [†]

Friedrich Schiller-Universität Jena, 07743 Jena, Germany

Thomas Stöhlker

Friedrich Schiller-Universität Jena, 07743 Jena, Germany;
Helmholtz-Institut Jena, 07743 Jena, Germany;
and GSI Helmholtzzentrum für Schwerionenforschung, 64291 Darmstadt, Germany

Manuel Vogel

GSI Helmholtzzentrum für Schwerionenforschung, 64291 Darmstadt, Germany

We have performed systematic measurements of the resistive cooling behavior of bunches of highly charged ions in a Penning trap after injection from an external source. In particular, we have been able to measure the exponential cooling rate of the axial center-of-mass motion and experimentally show its linear dependence on the ion number within the bunch, as expected from theory. The common center-of-mass energy of the ions is reduced by more than four orders of magnitude on the time scale of milliseconds while the single-ion cooling occurs on the scale of seconds, representing a highly effective way to remove the dominating part of the ion kinetic energy.

I. INTRODUCTION

Resistive cooling is a well-established technique to reduce the kinetic energy of charged particles that are confined in a Penning trap [1–5]. It reduces both the particle velocity and amplitude of oscillation, which is beneficial for a large number of applications, mainly with respect to precision measurements but also well-defined confinement close to the trap center [4,5]. The method is based on image currents that are induced by the particle motion [6,7] and attenuated by an electric impedance [1,3,5]. Most commonly, it is applied to the axial motion of the particles by a resonant electronic circuit that is tuned to their oscillation frequency, and that equilibrates the electronic temperatures of the circuit and the axial particle motion on a time scale given by properties of the arrangement [8].

For a single particle, as long as the electronic noise of the cooling circuit is much smaller than the signal induced by the particle motion, this results in an exponential decay of the axial particle kinetic energy [5,8]. The cooling rate γ_1 is given by the inverse of the observed cooling time constant of the exponential decay.

For an ensemble of N (identical) particles, the expected rate of cooling depends on the phase relation between the particles: for axial oscillations with random phases (e.g., a completely thermalized ensemble), the overall cooling rate is expected to be identical to the single-particle value γ_1 [1,3,5,9]. However, for an axial oscillation with a common phase (e.g., the center of mass of a confined ensemble), it is expected to be much higher, namely $N \cdot \gamma_1$, which may be several orders of magnitude faster than γ_1 [1,3,5,9].

In the following, we present measurements with highly charged ion bunches that are injected into the Penning trap of the HILITE experiment [10] and are resistively cooled by a dedicated resonant circuit tuned to the axial frequency. We experimentally show that with careful preparation of the injected ion bunches, the axial center-of-mass energy is by far the dominant contribution to the total ion energy, and that it can be reduced by more than 99.99% of its initial value on the time scale of milliseconds. At present, this is a rate advantage of a factor $N \sim 10^4$ when compared to measurements of resistive many-ion cooling with thermalized ion ensembles [11,12]. This is a quantitative study of the fast exponential center-of-mass cooling and its scaling with the number of ions over a considerable range, in agreement with a simple model of the cooling process.

---
[*]markus.kiffer@uni-jena.de

[†]stefan.ringleb@uni-jena.de

II. RESISTIVE COOLING AND ITS EXPERIMENTAL OBSERVABILITY

In the absence of cooling, the axial motion of a particle with charge q and mass m in an ideal Penning trap is described

by the differential equation [2,4,5]

$$\ddot{z} + \omega_z^2 z = 0, \tag{1}$$

where z is the axial coordinate, such that the particle performs a harmonic oscillation around the trap center at $z = 0$. The axial oscillation frequency ω_z is given by [2,4,5]

$$\omega_z = \sqrt{\frac{qU_0 C'}{md^2}}, \tag{2}$$

where U_0 is the trap voltage that constitutes the axial trapping potential U and d is the so-called characteristic trap size [2,5]. The quantities C' and d describe the relative voltage configuration of the Penning trap and its geometry, respectively. Presently, we have $C' = 1.0394$ and $d = 9.083$ mm. In an ideal Penning trap with its harmonic trapping potential $U \sim z^2$, the axial frequency ω_z is independent of the axial particle energy E_z, and the amplitude of the axial motion is proportional to the square root of E_z [4,5].

During its axial oscillation, a particle moves with respect to a given electrode and induces a fraction of its charge q as a so-called mirror charge inside of it [13]. Due to the particle motion, this leads to a current I (Shockley-Ramo theorem [6,7]) that is given by

$$I(t) = -\frac{q}{D}\dot{z}(t), \quad \text{with} \quad D = \left(\frac{\partial \Phi}{\partial z}\right)^{-1}, \tag{3}$$

where Φ is the normalized electric potential of the electrode in question. The quantity D is called the effective electrode distance of the dedicated pick-up electrode. It measures the separation required in an imagined pair of infinite parallel plates that effects to the same induced current between the plates as in the case of the given electrode with respect to ground [5]. As Eq. (3) shows, D depends on the geometry of the trap assembly and the position of the charged particle, it can be calculated from the electric potential Φ.

The induced current $I(t)$ can be used to detect and cool the axial particle motion. To this end, an RLC resonant circuit is connected to the electrode and the current produces a voltage $U(t) = ZI(t)$ across its complex impedance Z. This voltage is detected and used as a measure of the particle kinetic energy [1]. At the same time, the current $I(t)$ through the impedance leads to energy dissipation in the form of heat with power $P(t) = ZI^2(t)$ that is absorbed by the cryogenic surrounding and thus drains kinetic energy from the axial particle motion (resistive cooling). A suitable heat sink, at least for small numbers of particles, may alternatively be provided by coupling the RLC circuit to separately trapped particles that are cooled by other means such as, e.g., laser cooling [14,15].

The method of resistive cooling has been described in detail previously [1,3–5,8,9,16–18]. During resistive cooling, the particle kinetic energy decays like

$$E(t) = E(0) \exp(-\gamma t) \tag{4}$$

until an equilibrium is reached between the circuit's noise temperature and the temperature corresponding to the particle energy [4,5,8]. For a single particle, γ is the single-particle value γ_1 that is given by

$$\gamma_1 = \frac{q^2 R}{D^2 m}, \tag{5}$$

where R is the real part of the RLC circuit's impedance Z at the axial oscillation frequency ω_z. When the RLC resonance frequency ω_R is identical to ω_z, the acting impedance is purely Ohmic and takes the value $Z = R = QL\omega_R$, where L is the circuit's inductance and Q its quality factor [19].

In strong contrast to single-particle cooling at a rate γ_1 that is commonly of the order of a fraction of Hz to several Hz [4,5,16,20], the cooling of the center-of-mass (CM) motion of a particle ensemble has an expected rate of

$$\gamma = \gamma_1 N, \tag{6}$$

which may be several orders of magnitude faster than γ_1. In order to be able to directly observe the exponential decay of the center-of-mass energy, three conditions need to be fulfilled:

(i) The time resolution of the measurement needs to be better than $1/\gamma$;

(ii) There must be a sufficient amount of energy within the CM mode to be able to track its time evolution;

(iii) Energy exchange with other motional degrees of freedom needs to be negligible.

Previous dedicated measurements of resistive cooling of ion ensembles in Penning traps have taken place under conditions that were not favorable for the present observations. In particular, when the ion ensemble is close to thermalization initially, only a negligible fraction of its kinetic energy is in the CM mode, such that condition (ii) is not met, see, for example, Refs. [5,11,16,20]. Also, when significant amounts of energy from radial motion of the ions are transferred into or from the axial motion, the observed axial decay rate may be obscured and condition (iii) is violated. This leads to nonexponential decay as has been observed and discussed in detail in Refs. [5,12,16]. At present, since the ions upon their capture into the trap are one nearly monoenergetic bunch, the CM mode is dominant when compared to the relative axial and radial motions. Hence, the CM cooling can be observed as long as N is small enough not to violate condition (i). For the present ion numbers of up to several tens of thousands, condition (i) is fulfilled.

III. SETUP AND PROCEDURES

A. Penning trap

For the present measurements, we use a Penning trap inside a magnetic field of up to 6 T that is produced by a horizontal-bore superconducting magnet with a harmonic region of 10 mm in the center around $z = 0$. The electrode stack shown in Fig. 1 consists of seven central electrodes that constitute the trap and one additional electrode on either side to decelerate the ions and compress the ion bunch axially. The central ring electrode is split into eight identical segments. The trap is located in the center of the magnetic field, with its z axis falling together with the central axis of the magnetic field. The end-cap electrodes have a separation of 22.4 mm, and the inner diameter of the trap is 15 mm. The end caps have a central hole with a diameter of 4 mm to allow for loading the trap with externally produced ions [21] and axial ejection of the trap content. By using a set of seven trap electrodes, we have an additional degree of freedom compared to five-pole traps that consist of a ring electrode, two correction electrodes,
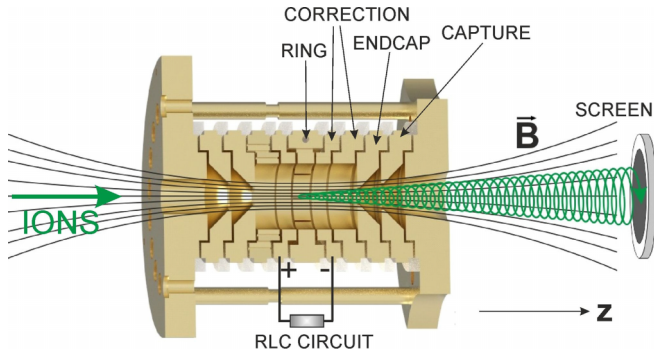
FIG. 1. Sectional drawing of the Penning trap. The trapping potential is created by the seven central electrodes (ring, four correction electrodes, and two end caps), the outer electrodes support the ion capture process. The trap has mirror symmetry with respect to its center, so only one half is labeled. The RLC circuit is connected to both inner correction electrodes, which are labeled with + and −.

and two end-cap electrodes [22]. This allows for tuning out the trapping potential imperfections of orders z^4 and z^6 simultaneously purely by choice of voltages. Table I shows the relative voltages required for a harmonic potential. The voltage source is capable of setting voltages of up to 400 V with respect to ground with a voltage resolution of 0.0125 V. The entire set of electrodes can be biased against ground by a voltage U_f for additional deceleration of incoming ions. The whole trap arrangement and cooling and detection electronics is cooled close to liquid-helium temperature by a pulse-tube cryocooler, making the RLC circuit an effective heat sink for resistive cooling. At the same time, it ensures efficient cryopumping such that charge exchange of the ions with neutral gas is not observed on the present time scales.

B. Ion capture into the trap

The present measurements are performed with Ne^{8+} ions (heliumlike neon) from a commercial electron-beam ion trap (EBIT) [23] that can deliver several tens of thousands of such ions per extraction pulse. The choice of this ion species is guided mainly by practical considerations and the expected results are qualitatively independent of this choice. The ions are extracted with a kinetic energy of 1895 eV per charge and deflected onto the central axis of the trap setup. An overview is shown in Ref. [10]. The distance between the deflection device and the ion trap is about 2 m. The ions are aligned with the magnetic field axis by a set of so-called Sikler lenses [24]. These lenses are fourfold-segmented ion-optical lenses, which can be used both to focus the ion beam and to steer it in the lateral direction. The ions are then decelerated by two

TABLE I. Relative electrode voltages for a harmonic potential. The ring electrode is set to 0 V.

Electrodes	Applied voltage
Inner correction	$0.059\,U_0$
Outer correction	$0.434\,U_0$
End cap	$1.000\,U_0$

pulsed drift tubes, the second of which has a crown-shaped structure comparable to the one described in Ref. [25]. With this configuration, the ion bunch is compressed axially to reduce its axial extent and axial energy distribution. When the ions enter the trap for dynamic capture [21], the first end-cap electrode is set to zero potential to allow the ions to enter across a low potential barrier. Then the end-cap electrode is switched to 95% of its final voltage with a rise time of about 200 ns. The full trap voltage is achieved after about 10 ms.

C. Detection system

For the present measurements, we use destructive and nondestructive ion detectors, namely:

(i) a nondestructive single-pass charge counter with a signal amplitude directly proportional to the number of ions in a passing ion bunch [26,27].

(ii) a microchannel plate (MCP) with a fluorescence screen that yields spatial information about the ejected ions and their time of flight from the trap to the detector.

(iii) a normal-conducting RLC resonant circuit with a subsequent low-noise cryogenic amplifier to detect the ions nondestructively in the ion trap.

1. Charge counter

To determine the number of ions in an ion bunch, we use a charge counter based on the amplification of mirror charges. This is a nondestructive technique, and the ion bunch can be characterized concerning ion number, ion energy, and bunch length within a single pass. The working principle and characterization methods are described in detail in Refs. [26,27]. The most important measurement here concerns the absolute number of ions N, which is determined from the relation

$$N = \frac{V_{\max}}{q \cdot S},\qquad(7)$$

where $V_{\max}$ is the measured peak voltage of the charge counter signal, q the charge of a single ion and S the sensitivity of the charge counter, which has been measured to be $S = \frac{\alpha}{C_{\det}} = 1800(71)\,\mathrm{nV\,e^{-1}}$.

To calibrate the detector we measured both the capacitance $C_{\det}$ of the assembled pickup electrode and the overall amplification factor α at room temperature. At the working temperature of 52 K the amplification factor of the amplifier will increase significantly. To determine the resulting value of S we applied a capacitively coupled harmonic signal both at room temperature and under cryogenic conditions. The relative increase of the sensitivity is given by the relative increase in the measured amplitude. For the present conditions, the counting accuracy is better than 10%.

2. Fluorescence MCP

We use a MCP with a fluorescence screen to obtain timing, quantity, and spatial distribution information of the ion bunch upon its ejection from the trap:

(i) Time-of-flight information is given by the MCP signal relative to ion ejection from the trap, see Fig. 2 top.

(ii) For fixed ion energy and MCP voltage, the area Ω_{MCP} of the MCP signal (see Fig. 2, top) is proportional to the
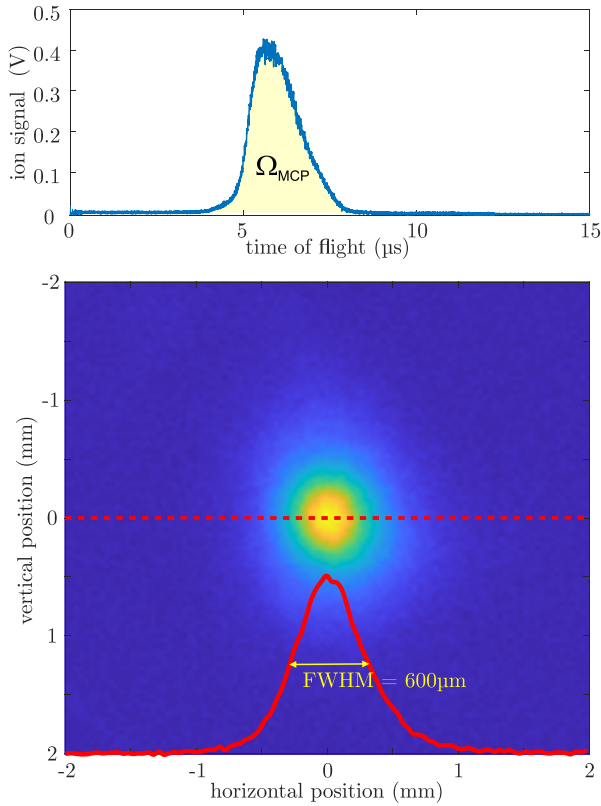
FIG. 2. Top: Ion signal on the MCP as a function of time with the peak area $\Omega_{MCP} \sim N$. Bottom: Measured radial ion distribution in the trap as visualised by the MCP fluorescence screen. The scaling of the axes is given by Eq. (8).

number of ions N, as we have verified by calibration with the charge counter.

(iii) From the spatial distribution of the ions on the MCP fluorescence screen as recorded by a CCD camera we can deduce the radial position of the ions at the moment of ion ejection from the trap.

The divergence of the magnetic field as depicted in Fig. 1 leads to a defined widening of the ions' radial motion between the trap and the MCP screen given by [28]

$$r_{MCP} = \sqrt{\frac{B_{trap}}{B_{MCP}}} r_{trap}, \qquad (8)$$

where B_{trap} and B_{MCP} are the magnetic field strengths in the trap center and at the position of the MCP detector, respectively. Hence, r_{trap} can be calculated from the measured r_{MCP}, presently $\sqrt{B_{trap}/B_{MCP}} \approx 4.38$.

The fluorescence image is used to optimize the ion injection on the central z axis, hence avoiding undesired effects from off-axis capture such as large initial radial motion. Figure 2 shows on-axis ion injection resulting in a Gaussian ion distribution around the trap center with a width (FWHM) of $600\,\mu m$ ($\sigma = 255\,\mu m$) as used for the present measurements. This corresponds to an average distance from the trap center of $112\,\mu m$ for the inner 95% of the ions.

TABLE II. Capacitance C_{tot}, inductance L and series resistivity R_S of the normal-conducting resonant circuit.

C_{tot}/pF	21.51(69)
$L/\mu H$	592(19)
R_S/Ω	141.20(57)

3. Resonant RLC circuit

We use a normal-conducting resonant circuit made of high-purity copper wire that is wound around a toroidal core made of polytetrafluorethylene (PTFE). The resonator circuit connects the two inner correction electrodes of the trap, see also Fig. 1.

We have separately measured the overall inductance $L = 592(20)\,\mu H$ of the circuit and have recorded the response curve of the resonator. From the obtained quality factor $Q = 37.16(31)$ and the central frequency $f = 1.410510(200)$ MHz we have determined its characteristic values given in Table II. When compared to superconducting circuits [29,30], where quality factors of several thousands are possible, the determined quality factor of our normal-conducting resonator is much smaller. However, in the present case of ion ensembles with several 10^4–10^5 charges, the signal strength and hence the cooling power is sufficiently high and does not come with requirements to maintain superconductivity. Also, the comparably large resonator width of $f/Q \approx 35$ KHz makes the detection and cooling insensitive to axial frequency shifts due to residual trap imperfections at the presently high initial ion energies.

D. Effective electrode distance D

The effective electrode distance D as used to determine the induced current I in Eq. (3) is presently given by

$$D = \left(\frac{\partial \Phi_+}{\partial z} - \frac{\partial \Phi_-}{\partial z}\right)^{-1}, \qquad (9)$$

where $+$ and $-$ label the respective electrode as shown in Fig. 1. We have used the COMSOL multiphysics FEM solver to calculate the electric potentials and electric fields of the electrodes and determine the effective electrode distance D from these fields. It depends on the position of the ions relative to the trap center. The z dependence of D can be seen in Fig. 3. The curve is symmetric around $z = 0$ because both opposing inner correction electrodes are used to pick up induced current. In the trap center, D has a value of 12.5 mm. For larger z, the value of D increases, which results in a weaker coupling between the detection electrodes and the ion motion. This is presently of relevance, as we are trapping ions with a high axial energy of approximately 30 eV per charge and ion, as was verified by lowering the trap voltage U_0 until significant losses from the trap were observed. This means that the size and motional amplitude of the ion cloud requires an appropriate average of D over all relevant ion locations.

In Ref. [11], the average value D_{avr} was determined by taking the mean value of D^2 over the estimated radial ion cloud distribution. Figure 3(a) shows that in the present experiment, the small radial ion extension of well below 1 mm
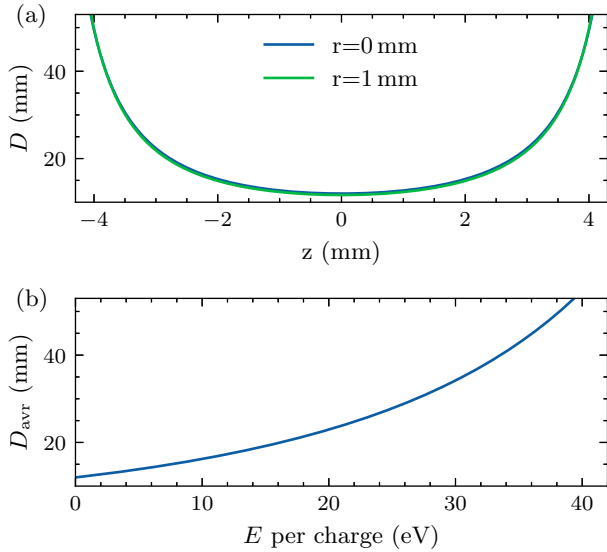
FIG. 3. (a) z dependence of the effective electrode distance D plotted for radial positions $r = 0$ and 1 mm, to show that small r have no influence on D. (b) energy dependence of D_{avr} due to the amplitude of the axial motion in the trap. D_{avr} was determined by a time average of $D(z)$ over a period of axial oscillation.

has no effect on D. However, to account for the strong axial dependence of D we have performed a time average of D over a period of axial oscillation. The time average is calculated by

$$D_{avr} = \left\langle \frac{1}{D(z_0 \cos(\omega_z t))} \right\rangle^{-1}, \tag{10}$$

where $z_0 = \sqrt{2E_z/(m\omega_z^2)}$ is the maximum axial amplitude of the ion motion. Figure 3(b) shows that the effect of the nonzero axial energy: For the present initial ion energy of 30 eV we estimate an average D of $D_{avr} \approx 33$ mm, which is much larger than the low-energy value of 12.5 mm.

IV. RESULTS

A. Resistive cooling

Directly upon capture, an ion bunch is stored in the Penning trap and the signal induced in the RLC circuit is measured. We have performed the measurement with a spectrum analyzer in the zero-span mode, i.e., the device performs a time-span measurement of the induced power $P(t) \sim I(t)^2 \sim E_{cm}$ in a small frequency window $\Delta f = 1$ kHz around a center frequency. This is sufficient to cover all frequency shifts due to cooling and potential fluctuations in the initial state of the created ion cloud and sufficiently small to suppress background noise. The zero-span scan is triggered such that the measurement starts immediately upon capture. Before each measurement of a cooling curve, we have performed an independent measurement of the axial frequency of the ion bunch to set the center frequency of the spectrum analyzer to this individual frequency.

Figure 4 shows an example of a recorded trace of the induced power $P(t)$ for Ne^{8+} ions in resonance with the RLC circuit. Initially, the signal rises within 20 ms to its maximum value. This is slower than the expected charging time of the
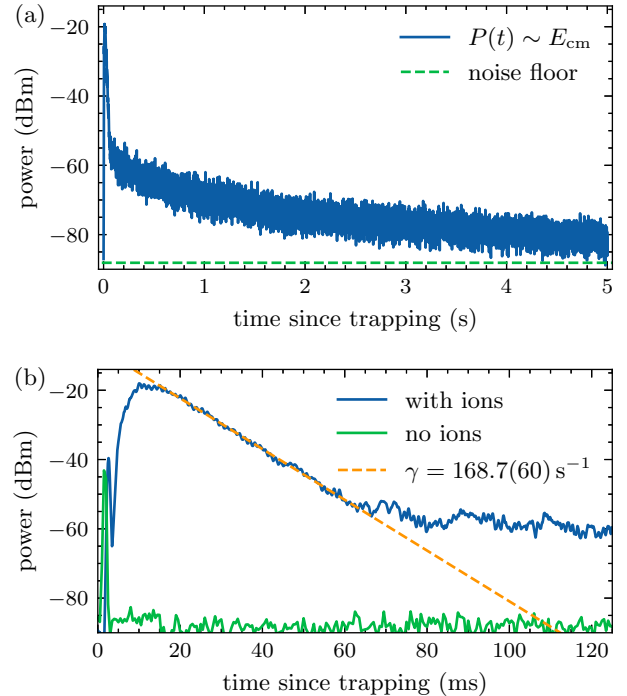

FIG. 4. Induced power $P(t)$ as a function of time for $N = 35000 \pm 3000$: (a) Logarithmic plot of $P(t)$ up to $t=5$ s and comparison with noise floor. (b) Zoomed-in view of the first 120 ms with an exponential decay fitted to the initial fast axial cooling. A reference measurement without ions shows the noise floor.

RLC circuit of about 50 µs, which we attribute to the time required to reach the full trap voltage and the axial ion frequency to come into the measurement window. From then on, the observed axial energy decays within 40 ms by a factor of about 15000, which can be described very well by an exponential decay with a decay time constant of presently 5.928(60) ms that corresponds to a rate of $\gamma = 168.7(60)\,\text{s}^{-1}$. This is mainly attributed to resistive cooling of the center-of-mass mode of the axial ion motion. After this initial fast decay, we observe a decay of $P(t)$ on much longer time scales. During this decay the signal is well above the noise level indicated by the green dashed line. The details of these observations will be modeled and discussed below.

B. Scaling of CM cooling with the number of ions

The main expected feature of the CM cooling is the scaling of its rate with N. To investigate this, we have varied the number of injected ions by the chosen breeding time of the ion source. To determine the number of trapped ions we use the signal area Ω_{MCP} of the fluorescence MCP detector, which has been calibrated by use of the image charge detector. With this method we have varied the number of ions from 3500–35000 and measured decay curves as the one shown in Fig. 4.

Figure 5 shows the observed cooling rates as a function of the ion number (measured in units of Ω_{MCP}). The data verifies that the measured cooling rates scale as $\gamma \sim N$ for sufficiently large N, currently above $N \approx 8500\ (\Omega_{MCP} = 0.1\,\mu\text{Vs})$, which corroborates this being the center-of-mass cooling. For smaller ion numbers, the observed decay is faster than
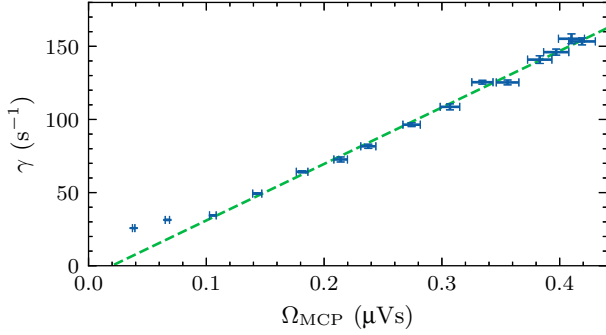
FIG. 5. Measured cooling rate as a function of the ion number in units of the MCP signal area $\Omega_{MCP} \sim N$. The dashed line is a linear fit to the data.

expected from $\gamma = N \cdot \gamma_1$. This can at present be explained by an additional decay mode with rate $\gamma_{ax} \approx 25\,s^{-1}$ that does not depend on the number of ions. We attribute this to the transfer of energy from the axial CM motion to uncorrelated axial motion, as will be justified by the model presented below.

C. Model for the cooling process

1. Description of the model

In this section, we discuss a model for resistive cooling based on Ref. [12], where it was used to interpret resistive cooling of ions with negligible CM energy. Here we apply the technique to a case where the ion cloud is far away from thermal equilibrium and the CM energy is dominant. In general we can split the motion of N trapped ions into three modes with a total of $3N$ degrees of freedom:

(i) the axial center-of-mass motion with a total energy of E_{cm} and one degree of freedom;

(ii) $N - 1$ degrees of freedom for the uncorrelated axial motions with total energy E_{ax};

(iii) $2N$ degrees of freedom for radial motions with total energy E_r.

The total kinetic energy E of the ion cloud is given by the sum of the three energies over all N ions. In our case the RLC circuit is connected to an axially symmetric set of electrodes. This means that on average the motion of the uncorrelated axial mode will not induce current in the resonator. Therefore, only the CM motion interacts with the RLC circuit and only E_{cm} is cooled restively. Due to this, the total energy E is cooled according to

$$\frac{dE}{dt} = \gamma_{cool}(E_{cm} - k_B T_0). \tag{11}$$

In principle, E can be cooled down to the ambient temperature T_0. We model energy transfer between the three modes according to the following diagram:

$$\boxed{T_0} \xleftarrow{\gamma_{cool}} \boxed{E_{cm}} \xleftrightarrow{\gamma_{ax}} \boxed{E_{ax}} \xleftrightarrow{\gamma_r} \boxed{E_r}$$
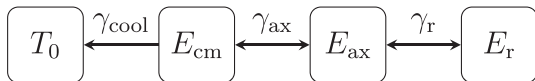
Each arrow shows the rate and direction at which energy is exchanged. Considering the individual degrees of freedom,

the set of rate equations is given by:

$$\frac{dE_{cm}}{dt} = -\gamma_{cool}(E_{cm} - k_B T_0) + \gamma_{ax}\left(\frac{1}{N-1}E_{ax} - E_{cm}\right)$$

$$\frac{dE_{ax}}{dt} = -\gamma_{ax}\left(\frac{1}{N-1}E_{ax} - E_{cm}\right) - \gamma_r\left(E_{ax} - \frac{N-1}{2N}E_r\right)$$

$$\frac{dE_r}{dt} = \gamma_r\left(E_{ax} - \frac{N-1}{2N}E_r\right). \tag{12}$$

The expected cooling rate γ_{cool} of the CM motion is given by $N \cdot \gamma_1$. The rate γ_{ax} is a result of the finite axial energy distribution of the trapped ions that in the presence of residual trap anharmonicities leads to a finite distribution of axial frequencies ω_z [2]. As a result, the relative phases of the axial ion motions change constantly, which represents an exchange of axial kinetic energy between the correlated motion E_{cm} and the uncorrelated mode E_{ax} [1].

To discuss the implications of the model we will, for now, neglect the radial mode, since γ_r is typically much smaller than γ_{cool} and γ_{ax}. In the case of the measured initial fast decay of E_{cm}, the ion cloud is far away from thermal equilibrium, i.e. $E_{cm} \gg E_{ax}/(N-1)$ and $E_{cm} \gg k_B T_0$. Thus the first rate equation simplifies to

$$\frac{dE_{cm}}{dt} = -(\gamma_{cool} + \gamma_{ax})E_{cm} = -\gamma E_{cm}. \tag{13}$$

This means that the observed decay rate γ of E_{cm} is given by the sum of γ_{cool} and γ_{ax}, which justifies the additional decay mode with γ_{ax} that was introduced in the discussion of Fig. 5.

After the fast initial cooling, the CM energy reaches a plateau. It is now in thermal equilibrium with the uncorrelated axial energy. The first rate equation shows that this is the case when $E_{cm} = E_{ax}/(N-1)$, which results in the following rate equation for the total energy:

$$\frac{dE}{dt} = \gamma_{cool}(E_{cm} - k_B T_0) = \frac{\gamma_{cool}}{N}(E - N k_B T_0). \tag{14}$$

This equation shows that, as expected, the total energy of an thermalized ion cloud cools with the single-particle cooling rate $\gamma_1 = \gamma_{cool}/N$. As this cooling takes longer than the recorded time, we do not expect any significant decay of E_{cm} from this point on. Hence, the value of the measured signal $P(t)$ at the plateau is a direct indicator of the remaining energy in the axial direction.

To describe the observed decay of E_{cm} at later times, it is necessary to consider the radial motion with energy E_r that couples to E_{ax} with rate γ_r. As Fig. 2 shows, the ion cloud is small and we can expect a small radial energy E_r. This means that energy can flow from E_{ax} into E_r with rate γ_r, which in turn results in slow decay of E_{cm}. This will continue until the radial and axial motions are in equilibrium [12]. In the present case of a large ensemble of highly charged ions in a well-tuned trap, we expect this to occur mainly through long-range ion-ion interactions, hence we estimate the equilibration rate from the Spitzer self-collision time [31]

$$\gamma_r^{-1} \approx t_s \approx (4\pi\epsilon_0)^2 \frac{3\sqrt{m}(k_B T)^{3/2}}{4\sqrt{\pi}nq^4 \ln\Lambda} \sim \frac{T^{3/2}}{n}, \tag{15}$$
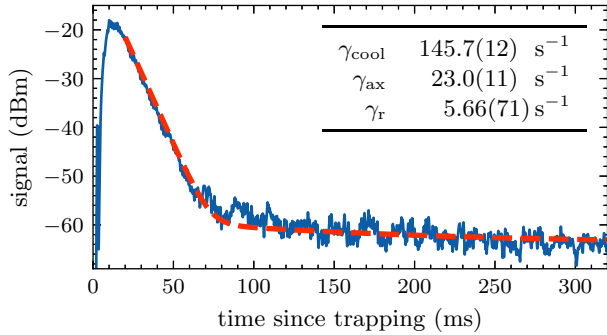
FIG. 6. Fit of the model for resistive cooling to the measured decay curve in Fig. 4. The modeled E_{cm} is scaled up and transformed to dBm to match the value for $t = 20$ ms. For the fit we only consider the time window from $t = 20$–320 ms. The resulting rates are shown in the figure and the energies are presented in Table III.

where n is the ion number density in the trap and $\ln \Lambda \approx 18$ is the Coulomb logarithm that only depends weakly on the temperature and the density. From the measured cloud radius and an axial ion energy of 30 eV per charge this results in $\gamma_r \approx 2 \, \text{s}^{-1}$.

2. Application to the data

We will now fit the free parameters of the model to the measured curve $P(t) \sim E_{cm}$ from Fig. 4. The calculated curve $E_{cm}(t)$ is scaled such that $E_{cm}(t)$ is numerically equal to $P(t)$ for $t = 20$ ms. This means that the resulting energies can only be expressed relative to the total energy E. The resulting energies and decay rates can be seen in Fig. 6 and Table III.

3. Interpretation of results

The fit results in the following conclusions for the determined decay rates:

(i) The fit result for the decay rate of E_{cm} given by $\gamma = \gamma_{cool} + \gamma_{ax} = 169.4(19) \, \text{s}^{-1}$ agrees well with the measured value of $168.7(60) \, \text{s}^{-1}$ as shown in Fig. 4(b).

(ii) The axial decay rate γ_{ax} agrees with the observed additional decay mode seen in the discussion of Fig. 5.

(iii) γ_r is of the correct order of magnitude such that the later slow decay can be explained by energy transfer from the axial motion to the radial motion.

This supports the validity of the presented model for resistive cooling even far away from thermal equilibrium. In this

TABLE III. Relative energies determined by fitting the model to the measured $P(t)$ curve. In thermal equilibrium the energy of each degree of freedom would be $\hat{e} = E/3N$, thus we present the energies in units of $\hat{e}$. In these units the ion cloud is in thermal equilibrium when all energies are equal to unity. The results is shown for $t = 20$ ms and $t = 300$ ms.

	20 ms	300 ms
$E_{cm}/\hat{e}$	2260(110)	0.16
$\frac{1}{N-1}E_{ax}/\hat{e}$	2.932(40)	1.18
$\frac{1}{2N}E_{r}/\hat{e}$	0.0017(17)	0.90

regime, it remains appropriate to look at the kinetic energies of the ions rather than assuming a temperature picture like in studies with thermalized ensembles [11,12]. Correspondingly, other than in those discussions, the ion cloud is in a weakly correlated state with a plasma parameter $\Gamma \ll 1$ [5].

Table III shows the resulting energies at the start and the end of the fit procedure. The energies are normalized such that in thermal equilibrium they are all equal to unity. In the column for 20 ms one can see that indeed the CM motion has the most energy per degree of freedom and the cloud is far away from thermal equilibrium initially. After 300 ms, the CM motion is cooled below thermal equilibrium with the other motions. This can be understood from the first rate equation, as the cooling of E_{cm} has to be considered as well. In this case equilibrium is reached when $\frac{d}{dt}E_{cm} = 0$, which results in $E_{cm}/\hat{e} < 1$. One can also see that the radial and axial motions have almost thermalized with each other. Due to the unknown behavior of the RLC circuit and its interaction with the ions before $t = 20$ ms, we can not extrapolate the model to $t = 0$.

V. SUMMARY AND OUTLOOK

We have measured the resistive cooling behavior of large ensembles of highly charged ions (Ne^{8+}) in a Penning trap. In contrast to previous many-ion measurements [11,12], the trapped ions' axial CM motion is far from equilibrium with the other modes of motion initially. In this situation, we have demonstrated the fast exponential cooling of the axial CM energy by a factor of 15000 within 60 ms after trapping. We have confirmed the expected linear scaling of the cooling rate γ with the ion number N for a wide range of ion numbers N that are large enough such that resistive CM cooling dominates over other decay paths. Thus, the CM energy of a large ion ensemble can be efficiently cooled on the time scale of milliseconds even with a normal-conducting resonator. This has implications for trap experiments that use an external ion source: By using a well-defined dynamic capture process, an ion bunch can be trapped directly in a highly harmonic potential such that a broadband RLC circuit cools the CM motion fast enough to avoid the decay into an uncorrelated motion.

We have used a model based on coupled rate equations to describe the exchange of energy between different motions in the ion cloud. From a successful fit of the model to the measured decay curve we have extracted the energy exchange rates. They are in agreement with the measurement and with the expected values. We have also determined the initial energy distribution and the distribution for the thermalized ion cloud. The presented measurements show the validity of this model of resistive cooling not only for thermalized ion ensembles [11,12], but also for an ion cloud far away from equilibrium.

We will use the demonstrated methods to minimize the final temperature of the ion cloud by optimizing the employed capture process. At present we are already able to trap the ion bunch without significant radial energy. By minimization of the measured plateau value we can also reduce the remaining axial energy and therefore the final temperature of the ion cloud.

[1] D. J. Wineland and H. G. Dehmelt, J. Appl. Phys. **46**, 919 (1975).

[2] L. S. Brown and G. Gabrielse, Rev. Mod. Phys. **58**, 233 (1986).

[3] W. M. Itano, J. C. Bergquist, J. J. Bollinger, and D. J. Wineland, Phys. Scr. **1995**, 106 (1995).

[4] G. Werth, V. N. Gheorghe, and F. G. Major, *Charged Particle Traps* (Springer, Heidelberg, 2005).

[5] M. Vogel, *Particle Confinement in Penning Traps* (Springer, Cham, 2018).

[6] W. Shockley, J. Appl. Phys. **9**, 635 (1938).

[7] S. Ramo, Proc. IRE **27**, 584 (1939).

[8] S. Djekic, J. Alonso, H.-J. Kluge, W. Quint, S. Stahl, T. Valenzuela, J. Verdu, M. Vogel, and G. Werth, Eur. Phys. J. D **31**, 451 (2004).

[9] P. Ghosh, *Ion Traps* (Oxford University Press, Oxford, 1995).

[10] S. Ringleb, N. Stallkamp, M. Kiffer, S. Kumar, J. Hofbrucker, B. Arndt, M. Vogel, W. Quint, T. Stöhlker, and G. G. Paulus, Phys. Scr. **97**, 084002 (2022).

[11] M. S. Ebrahimi, Z. Guo, M. Vogel, M. Wiesel, G. Birkl, and W. Quint, Phys. Rev. A **98**, 023423 (2018).

[12] M. Vogel, H. Häffner, K. Hermanspahn, S. Stahl, J. Steinmann, and W. Quint, Phys. Rev. A **90**, 043412 (2014).

[13] D. F. A. Winters, M. Vogel, D. Segal, and R. C. Thompson, J. Phys. B **39**, 3131 (2006).

[14] M. Bohman, V. Grunhofer, C. Smorra, M. Wiesinger, C. Will, M. J. Borchert, J. A. Devlin, S. Erlewein, M. Fleck, S. Gavranovic, J. Harrington, B. Latacz, A. Mooser, D. Popper, E. Wursten, K. Blaum, Y. Matsuda, C. Ospelkaus, W. Quint, J. Walz *et al.*, Nature (London) **596**, 514 (2021).

[15] C. Will, M. Bohman, T. Driscoll, M. Wiesinger, F. Abbass, M. J. Borchert, J. A. Devlin, S. Erlewein, M. Fleck, B. Latacz, R. Moller, A. Mooser, D. Popper, E. Wursten, K. Blaum, Y. Matsuda, C. Ospelkaus, W. Quint, J. Walz, C. Smorra, and S. Ulmer, New J. Phys. **24**, 033021 (2022).

[16] H. Häffner, T. Beier, S. Djekic, N. Hermanspahn, H.-J. Kluge, W. Quint, S. Stahl, J. Verdu, T. Valenzuela, and G. Werth, Eur. Phys. J. D **22**, 163 (2003).

[17] X. Feng, M. Charlton, M. Holzscheiter, R. A. Lewis, and Y. Yamazaki, J. Appl. Phys. **79**, 8 (1996).

[18] M. H. Holzscheiter, Phys. Scr. **1988**, 73 (1988).

[19] F. E. Terman, *Radio Engineers' Handbook* (McGraw-Hill, New York, 1943).

[20] L. Gruber, J. P. Holder, and D. Schneider, Phys. Scr. **71**, 60 (2005).

[21] H. Schnatz, G. Bollen, P. Dabkiewicz, P. Egelhof, F. Kern, H. Kalinowsky, L. Schweikhard, H. Stolzenberg, and H.-J. Kluge, Nucl. Instrum. Meth. Phys. Res. A **251**, 17 (1986).

[22] G. Gabrielse, L. Haarsma, and S. L. Rolston, Int. J. Mass Spectrom. Ion Processes **88**, 319 (1989).

[23] G. Zschornack, M. Kreller, V. P. Ovsyannikov, F. Grossman, U. Kentsch, M. Schmidt, F. Ullmann, and R. Heller, Rev. Sci. Instrum. **79**, 02A703 (2008).

[24] P. Mandal, G. Sikler, and M. Mukherjee, J. Instrum. **6**, P02004 (2011).

[25] L. Schmöger, M. Schwarz, T. M. Baumann, O. O. Versolato, B. Piest, T. Pfeifer, J. Ullrich, P. O. Schmidt, and J. R. C. López-Urrutia, Rev. Sci. Instrum. **86**, 103111 (2015).

[26] M. Kiffer, S. Ringleb, N. Stallkamp, B. Arndt, I. Blinov, S. Kumar, S. Stahl, T. Stöhlker, and M. Vogel, Rev. Sci. Instrum. **90**, 113301 (2019).

[27] S. Ringleb, M. Kiffer, J. K. C. Ballentin, T. Stöhlker, and M. Vogel, Sci. Rep. **13**, 22669 (2023).

[28] J. D. Jackson, *Classical Electrodynamics*, 3rd ed. (Wiley, New York, 1999).

[29] S. Ulmer, H. Kracke, K. Blaum, S. Kreim, A. Mooser, W. Quint, C. C. Rodegheri, and J. Walz, Rev. Sci. Instrum. **80**, 123302 (2009).

[30] M. S. Ebrahimi, N. Stallkamp, W. Quint, M. Wiesel, M. Vogel, A. Martin, and G. Birkl, Rev. Sci. Instrum. **87**, 075110 (2016).

[31] L. Spitzer, *Physics of Fully Ionized Gases* (Interscience, New York, 1956).